Applied Clay Science 55 (2012) 18–26

Contents lists available at SciVerse ScienceDirect

Applied Clay Science

journal homepage: www.elsevier.com/locate/clay

Morphology and composition controllable synthesis of Mg–Al–CO_3 hydrotalcites by tuning the synthesis pH and the CO_2 capture capacity

Qiang Wang [a,*], Hui Huang Tay [a], Zhanhu Guo [b], Luwei Chen [a], Yan Liu [a], Jie Chang [a], Ziyi Zhong [a], Jizhong Luo [a,**], Armando Borgna [a]

[a] Heterogeneous Catalysis, Institute of Chemical and Engineering Sciences (ICES), A*STAR, 1 Pesek Road, Jurong Island, 627833 Singapore
[b] Integrated Composites Laboratory, Dan F. Smith Department of Chemical Engineering, Lamar University, Beaumont, TX 77710 USA

ARTICLE INFO

Article history:
Received 23 April 2011
Received in revised form 29 July 2011
Accepted 30 July 2011
Available online 12 November 2011

Keywords:
Synthesis mechanism
Effect of pH
Layered double hydroxides
Isoelectric point
γ-AlOOH
Morphology

ABSTRACT

In order to achieve a controllable synthesis of hydrotalcites (HTs), a systematic investigation on the synthesis of Mg–Al HTs at different pH values was performed. The physical and chemical properties of the synthesized HTs were characterized by X-ray diffraction, scanning electron microscope, thermogravimetric analysis, differential scanning calorimetry, temperature programmed desorption, and BET. The chemical compositions were determined by inductively coupled plasma. The results revealed that the synthesis pH plays a crucial role on the morphology, pore structure and chemical composition of the final products. When the synthesis pH equaled to the isoelectric point (IEP) of Mg–Al HT, "rosette" morphology was formed; while when the pH was higher than the IEP, meso-porous HTs were synthesized. The inter-layered charge compensating anions as well as the Mg/Al ratio also varied with the synthesis pH. Based on our observations, a synthesis mechanism which describes the formation process under various synthesis conditions, was proposed. In addition, we have shown that this mechanism could also be applicable to other synthesis methods. Finally, the CO_2 adsorptions on these synthesized HTs were evaluated. It is clear that the synthesis conditions strongly affected the adsorption capacity. The highest capacity was obtained over the Mg_3Al_1–CO_3 (pH 12) sample, showing a CO_2 capture capacity of 0.83 mmol/g when pre-calcined for 1 h and 0.58 mmol/g when pre-calcined for 6 h, respectively.

1. Introduction

Hydrotalcites (HTs) have attracted an increasing interest because of their potential applications as CO_2 adsorbents, ion exchangers, fire retardants, base catalysts, and precursors of well-mixed oxides for various catalytic applications (Climent et al., 2010; Hutson and Attwood, 2008; Manzi-Nshuti et al., 2008; Montanari et al., 2010; Nyambo et al., 2008; Oliveira et al., 2008; Reijers et al., 2006; Takagaki et al., 2010; Wang et al., 2010a, 2010b; Wang et al., 2011a, 2011b). Their structures consist of positively charged brucite-like layers, with interlayer spaces containing charge compensating anions and water molecules. The metal cations occupy the centers of the octahedral structure, whose vertexes contain hydroxide ions and the octahedrons are connected by sharing edges with each other to form an infinite sheet. The general formula of these compounds is $[M^{2+}_{1-x}M^{3+}_x(OH)_2][A^{n-}]_{x/n}\cdot ZH_2O$, where M^{2+} and M^{3+} are divalent (Mg^{2+}, Zn^{2+}, Ni^{2+}, etc.) and trivalent (Al^{3+}, Ga^{3+}, Fe^{3+}, Mn^{3+}, etc.) cations respectively. A^{n-} is a non-framework charge compensating anion (CO_3^{2-}, Cl^-, SO_4^{2-}, etc.), and x is normally between 0.2 and 0.4 (Benito et al., 2010; Cavani et al., 1991; Costantino et al., 2009; Du and O'Hare, 2008; Herrero et al., 2009; Hu et al., 2007; Wang et al., 2009).

Due to their wide applications in energy and environmental fields, HTs have been extensively synthesized and studied for decades. Up to date, several synthesis methods including co-precipitation (Kagunya et al., 1996; Kovanda et al., 2003), urea hydrolysis (Costantino et al., 1998; Hibino and Ohya, 2009; Xu and Lu, 2005), structure reconstruction (so called memory effect) (Benito et al., 2008; Perez-Ramirez et al., 2007), sol–gel (Paredes et al., 2006), and ion exchange (Tamura et al., 2006; Tsujimura et al., 2007) among others, have been well developed. In certain cases, in order to increase the crystalline degree or to control the morphology of HTs, the aging process can be further assisted by either hydrothermal treatment (Labajos et al., 1992), sonication (Climent et al., 2004), or microwave irradiation (Benito et al., 2007; Komarneni et al., 1996). And under different synthesis conditions, HTs with various morphologies such as rosette (Wang et al., 2010a, 2010b), platelet-like (Benito et al., 2006; Ma et al., 2008), stone-like (Wang et al., 2011a, 2011b), and an agglomeration of irregular aggregates (Oliveira et al., 2008; Venugopal et al., 2009) have been reported. However, despite the significant progress achieved on the preparation of HTs, detailed knowledge on the control of the microstructure, morphology, and chemical composition of HTs is still limited. Thus, further studies on

* Correspondence to: Q. Wang, Chemistry Research Laboratory, Department of Chemistry, University of Oxford, Mansfield Road, Oxford, OX1 3TA, United Kingdom.
** Corresponding author.
E-mail addresses: qiang.wang.ox@gmail.com (Q. Wang), luo_jizhong@ices.a-star.edu.sg (J. Luo).

0169-1317/$ – see front matter © 2011 Elsevier B.V. All rights reserved.
doi:10.1016/j.clay.2011.07.024

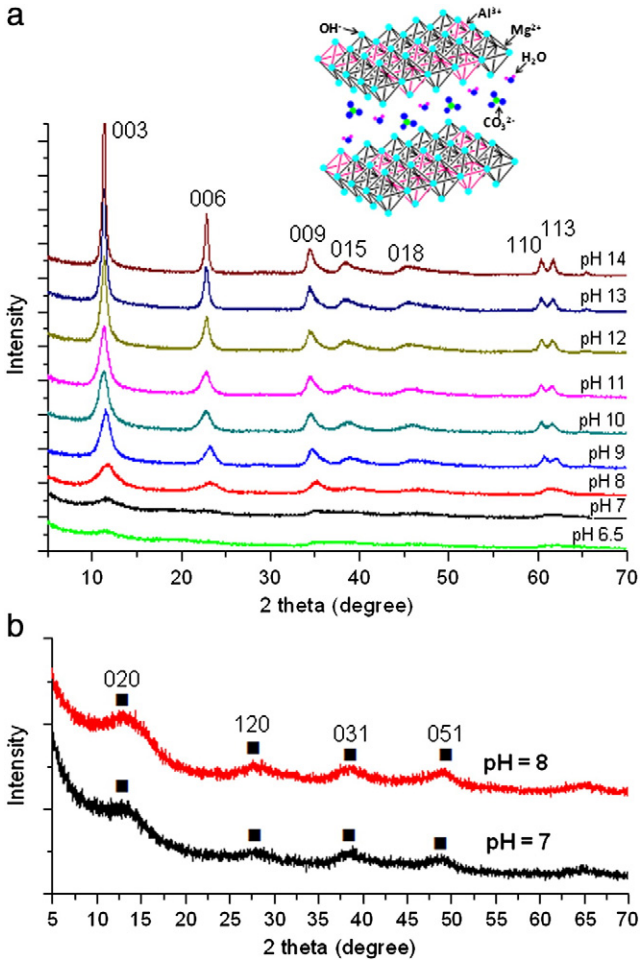

Fig. 1. (a) XRD patterns synthesized Mg–Al HTs at different pH values. The inset shows the schematic structure of Mg–Al–CO_3 HT; (b) XRD patterns of samples synthesized by adding $Al(NO_3)_3$ solution drop-wise into Na_2CO_3 solution, accompanied by controlling the pH at 7 and 8 using NaOH solution.

the controlled synthesis of HTs are still necessary (Wang et al., 2010a, 2010b; Xu and Lu, 2005).

In order to understand the synthesis process, many mechanisms have been proposed. For instance, Xu et al. (Xu and Lu, 2005) proposed a dissociation–deposition–diffusion mechanism by synthesizing HTs from MgO and Al_2O_3. They proved that the formation of HTs can be originated either from Al_2O_3 ($Al(OH)_3$) or MgO ($Mg(OH)_2$) mother structures. Boclair and coworkers investigated the synthesis mechanism through observation of the titration process of M^{2+} and M^{3+} with NaOH. The general procedure consisted of adding NaOH solution drop-wise into a metal precursor solution (Boclair et al., 1999; Boclair and Braterman, 1999). The M^{3+} hydroxide/hydrous oxide intermediates were formed in the low pH region; and further addition of NaOH resulted in the

Table 1
Characterizations of HTs samples synthesized at pH 6.5–14.

pH	*a* (Å)	*c* (Å)	Crysize L (nm)	Lvol-IB (nm)	Mg/Al molar ratio
6.5	3.051	26.267	1.8	1.16	0.5
7.0	3.045	25.168	2.2	1.40	0.6
8.0	3.043	23.709	3.5	2.20	1.5
9.0	3.046	23.319	5.8	3.71	2.3
10.0	3.057	23.502	6.3	4.03	3.1
11.0	3.057	23.584	7.3	4.66	3.1
12.0	3.056	23.471	9.80	6.26	3.2
13.0	3.056	23.318	15.4	9.83	3.2
14.0	3.057	23.269	23.7	15.06	3.2

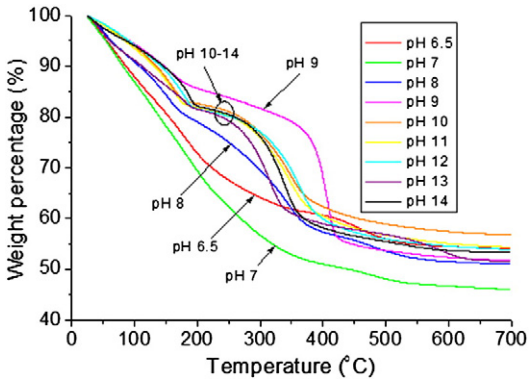

Fig. 2. TGA analyses of HTs synthesized at different pHs.

the pH values increased throughout the above titration process, the final HT products (co-precipitation method) were a mixture of irregular aggregates (Boclair et al., 1999; Boclair and Braterman, 1999; Seron and Delorme, 2008). In order to have a deeper understanding of the HT formation mechanism and a much better control of the HT products, a systematic study of the synthesis of Mg–Al HTs via the traditional co-precipitation method at a series of constant pH values ranging from 6.5 to 14 is reported in this contribution. The synthesized HTs samples were then characterized by X-ray diffraction (XRD), scanning electron microscope (SEM), thermogravimetric analysis (TGA), differential scanning calorimetry (DSC), temperature programmed desorption (TPD), and BET. The chemical composition of the HTs was determined using inductively coupled plasma (ICP). Using controlled synthesis conditions, the morphology, pore structure and chemical composition can be successfully tuned. By correlating the synthesis pH and the structures, plausible formation mechanism was proposed. The feasibility of the proposed mechanism was further verified by obtaining additional supporting evidence using hydrothermal synthesis method. Since HTs are promising high-temperature CO_2 adsorbents, the CO_2 capture properties of these HT samples were also investigated.

2. Experimental section

2.1. Preparation of HTs

All chemicals were purchased from Merk KGaA(Germany) and Sigma-Aldrich(USA). The general procedures of the co-precipitation method have been described elsewhere (Wang et al., 2010a, 2010b). In brief, a salt solution A (100 ml) containing a mixture of 0.075 mol Mg $(NO_3)_2 \cdot 6H_2O$ and 0.025 mol $Al(NO_3)_3 \cdot 9H_2O$ was added drop-wise to a basic solution B (100 ml) containing 0.05 mol Na_2CO_3. The pH value of solution B was kept constant (6.5–14) by addition of a solution C (50 ml) containing 0.17 mol NaOH. The resulting mixture D was aged at room temperature for 24 h with continuous stirring. The aged mixture was filtered and washed with deionized water until pH = 7, followed by drying at 100 °C in an oven. Hydrothermal synthesis was performed by placing 40 ml of the mixture D into a 45 ml Teflon lined stainless steel autoclave and hydrothermally treated at 150 °C for 48 h. After hydrothermal aging, the sample was filtered and dried at 100 °C in an oven.

2.2. Characterization of HTs

The BET specific surface areas were measured from the N_2 adsorption and desorption isotherms at 77 K collected using a Quantachrome Autosorb-6B surface area and pore size analyzer. Before each measurement, fresh HTs were first degassed at 110 °C overnight. Powder XRD analyses were conducted in a Bruker D8 Advance X-ray diffractometer equipped with a RINT 2000 wide-angle goniometer using Cu Kα radiation and a power of 40 kV × 40 mA. Diffraction patterns were recorded within the range of 2θ = 5–70° with a step size of 0.02°. The

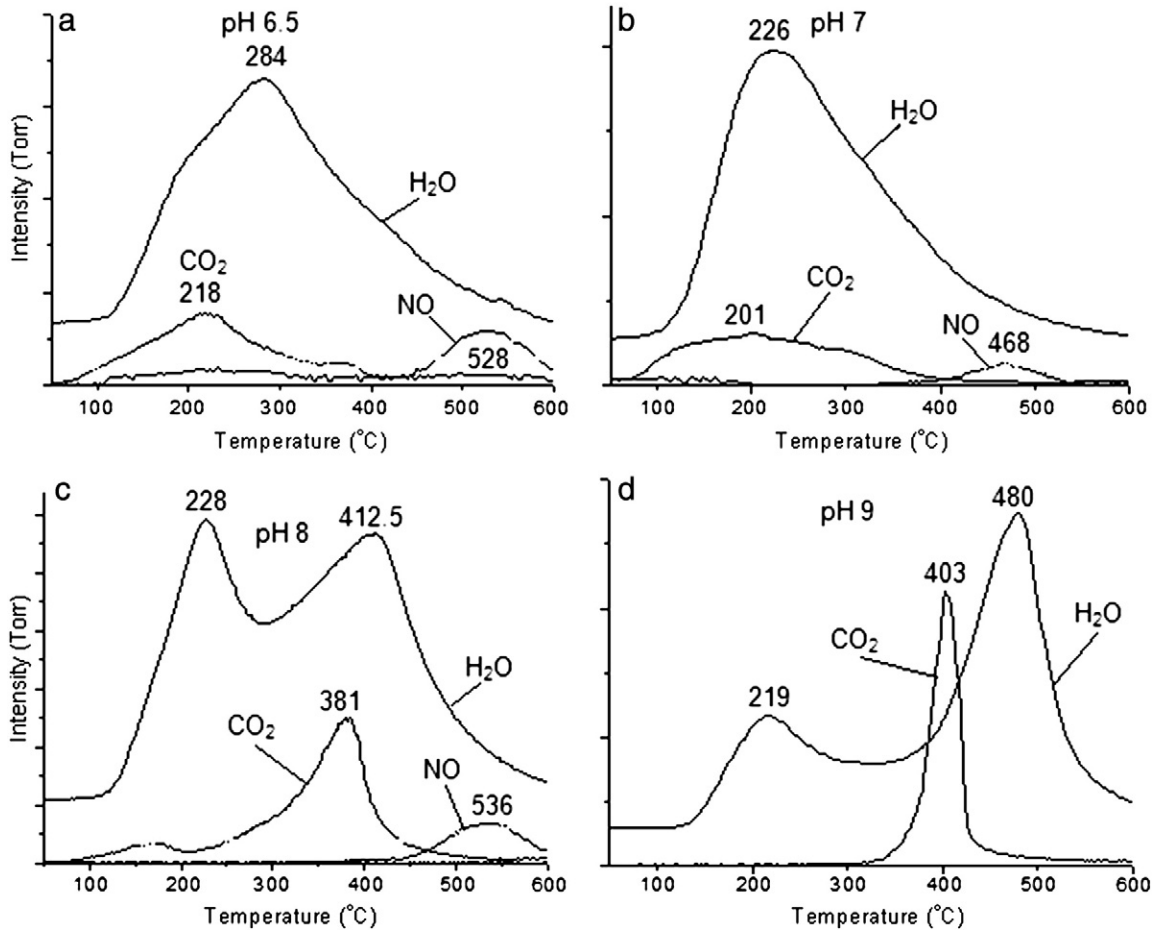

Fig. 3. TPD analyses of Mg–Al HTs synthesized at pH equals (a) 6.5, (b) 7, (c) 8, and (d) 9.

morphologies of synthesized HTs were observed using SEM (JEOL JSM-6700F). Before observation, the dried samples were sputtered and coated with gold, for ~120 s under argon atmosphere. During thermal treatment of HTs, the weight loss was determined using a TGA (Q500, TA Instruments, flow rate = 20 ml/min). Typically, about 10 mg sample was used for each run. The sample was heated in N_2 from 30 to 600 °C with a ramping rate of 5 °C/min. DSC analyses were performed using an automatic thermal analyzer (NETZSCH, DSC204 HP, USA). Sealed aluminum pans with pierced lids were used for all the samples and an empty pan prepared in the same way was used as a reference. 10 mg samples were weighted directly into the aluminum pans and the thermal analyses were conducted at a scanning rate of 5 °C/min from 50 to 450 °C. TPD experiments were conducted to monitor the decomposition of HTs. Fresh HTs (50 mg) were placed in a stainless steel reactor and heated from room temperature to 600 °C. The reactor was controlled by a proportional-integral-derivative (PID) temperature controller/programmer (Yudian Automation Enginering Co., Ltd, China), and the temperature was measured using a K-type thermocouple (0.5 mm outer diameter). Inert gas (Ar, 50 ml/min) was continuously fed into the reactor and the composition of the outlet gas was monitored by a mass spectrometer (HPR-20 QIC Atmospheric Gas Analysis System, UK). The elemental composition of the synthesized samples was analyzed by ICP-OES (Varian Vista-MPX CCD Simultaneous ICP-OES) after the samples were digested using aqua regia and kept in 2% HNO_3.

2.3. Evaluation of CO_2 capture capacity

Adsorption of CO_2 on HTs was measured using a thermogravimetric method on a Q500 TGA analyzer. Samples were pre-calcined at 400 °C for either 1 h or 6 h in Ar atmosphere before CO_2 adsorption experiments. To minimize potential errors caused by the memory effect, all experiments were carried out immediately after the first calcination. CO_2 adsorption experiments were carried out at 200 °C and 1 atm with a constant flow of CO_2 (40 ml/min).

3. Results and discussion

Fig. 1(a) shows the XRD patterns of HTs synthesized at various pH values ranging from 6.5 to 14. When the pH was lower than 8, the formation of HTs was not favored and the final products were most likely amorphous boehmite (γ-AlOOH). With the increase of pH from 8 to 14, the crystalline degree of synthesized HTs gradually increased. In the meantime, the layer distance d_{003} decreased with the increase in synthesis pH value (see Table 1). At pH ≥ 10, the lattice parameter *a* became stable (ca. 3.056–3.057 Å), indicating that the Mg/Al ratio should be similar for all these samples. Then, the Mg/Al ratios were analyzed by ICP-OES, and the values are shown in Table 1. With the increase of pH from 6.5 to 10, the Mg/Al ratio increased from a very small value of 0.5 to 3.1 (very close to the theoretical value 3). When the pH was higher than 10, the Mg/Al ratio kept constant at around 3.1–3.2, which is consistent with the XRD analysis. The inset of Fig. 1(a) shows the schematic structure of Mg–Al–CO_3 HT.

For the samples synthesized at pH 6.5–7, the Mg/Al ratios were only 0.5–0.6, indicating that only a small fraction of Mg–Al HTs was formed. To further confirm the composition of these products, another two samples were prepared by adding $Al(NO_3)_3$ solution drop-wise into Na_2CO_3 solution, accompanied by controlling the pH at 7–8 with NaOH solution. The XRD patterns of these two samples are shown in Fig. 1(b), from which the characteristic peaks of γ-AlOOH were observed at 12.8°, 27.9, 38.4, and 48.9 respectively (JCPDS 21–1307) (Chen et al., 2008).

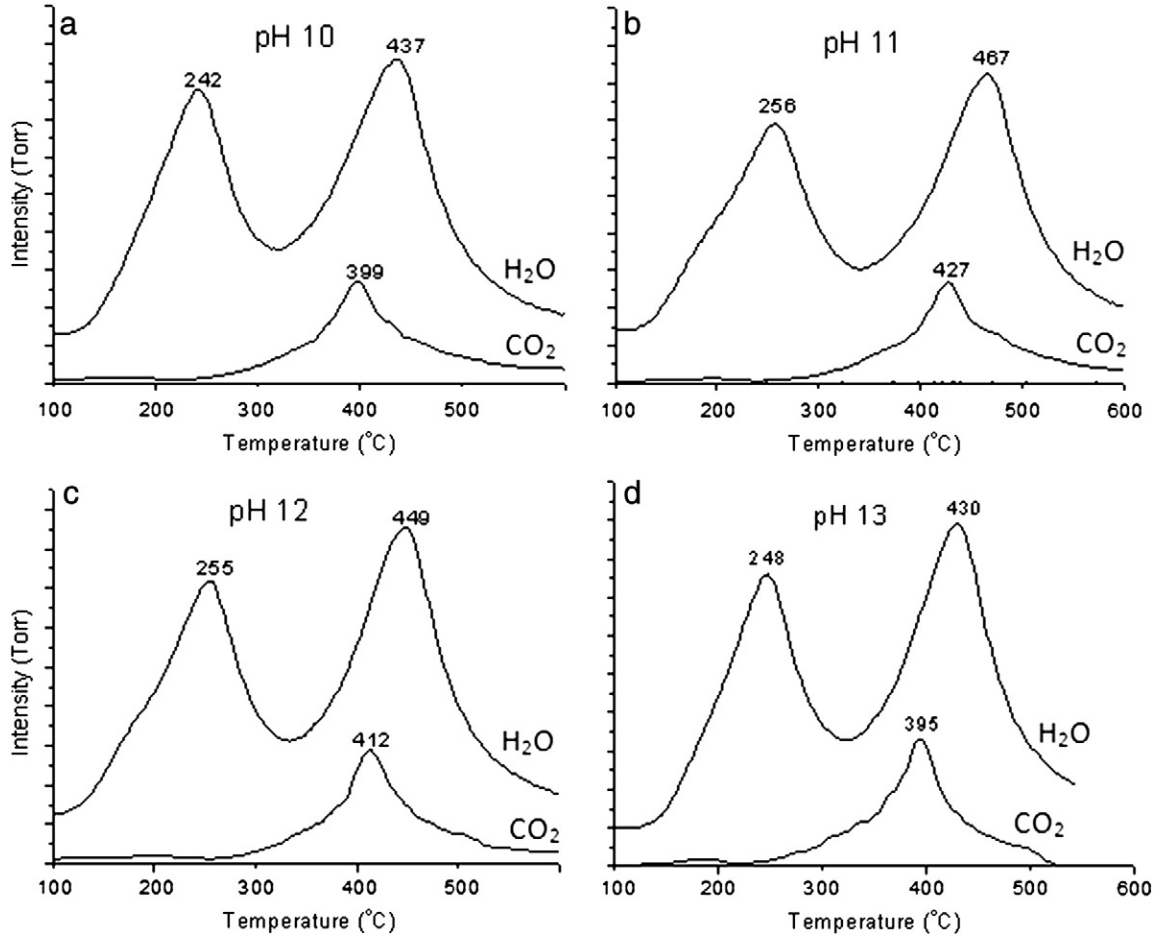

Fig. 4. TPD analyses of Mg–Al HTs synthesized at pH equals (a) 10, (b) 11, (c) 12, and (d) 13.

These results suggest that the samples synthesized at pH 6.5–7 are mainly γ-AlOOH together with small fraction of Mg–Al HT. TGA analysis in Fig. 2 and TPD analysis in Figs. 3 also confirmed this conclusion. When the synthesis pH = 6.5–7, the typical two-stage TGA profile for HTs was not observed, and there is only one H_2O desorption peak at around 227 °C in the TPD profiles. In Fig. 3(a) and (b), a NO peak was observed at around 468–528 °C, suggesting that the inter-layer charge compensating anions are probably NO_3^- for the samples synthesized at pH = 6.5–7. Another CO_2 peak at around 201–218 °C was also detected, and it might be due to the physically adsorbed CO_2 on γ-AlOOH. It is generally accepted that the decomposition temperature of the interlayer charge compensating anions is around 400 °C (Wang et al., 2011a, 2011b). However, it is still not clear whether this small portion of HT stays on the surface of γ-AlOOH or as separate particles.

For samples synthesized at pHs 8 and 9, the Mg/Al ratios increased to 1.5 and 2.3 respectively, but were still lower than the theoretical value of 3. Fig. 2 shows that the TGA profiles of these two samples begin to show the typical two-stage decomposition profile of HTs, suggesting that more HT phase was formed in these samples, as compared to those synthesized at pH 6.5–7. However, their TGA curves were still very

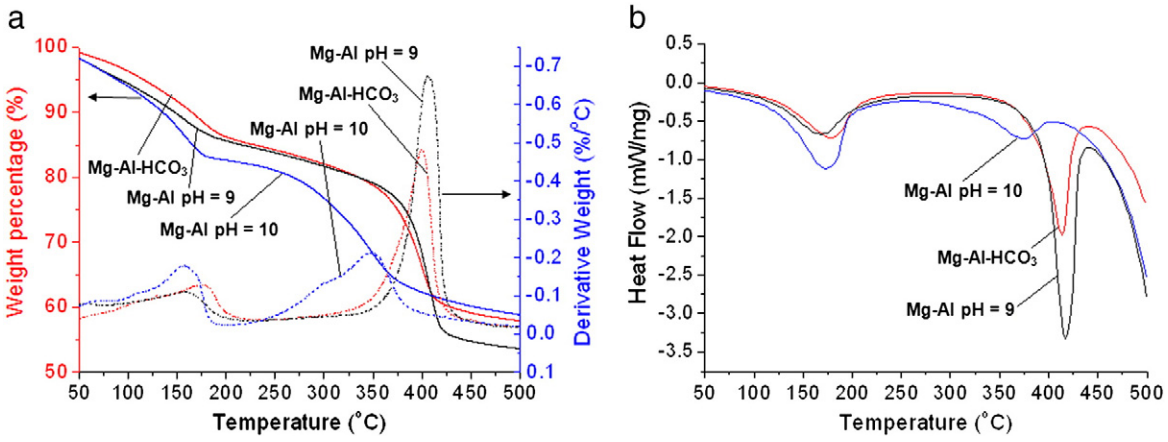

Fig. 5. (a) TGA analyses, (b) DSC analyses of Mg–Al–HCO_3, Mg–Al HT pH = 9, and Mg–Al HT pH = 10.

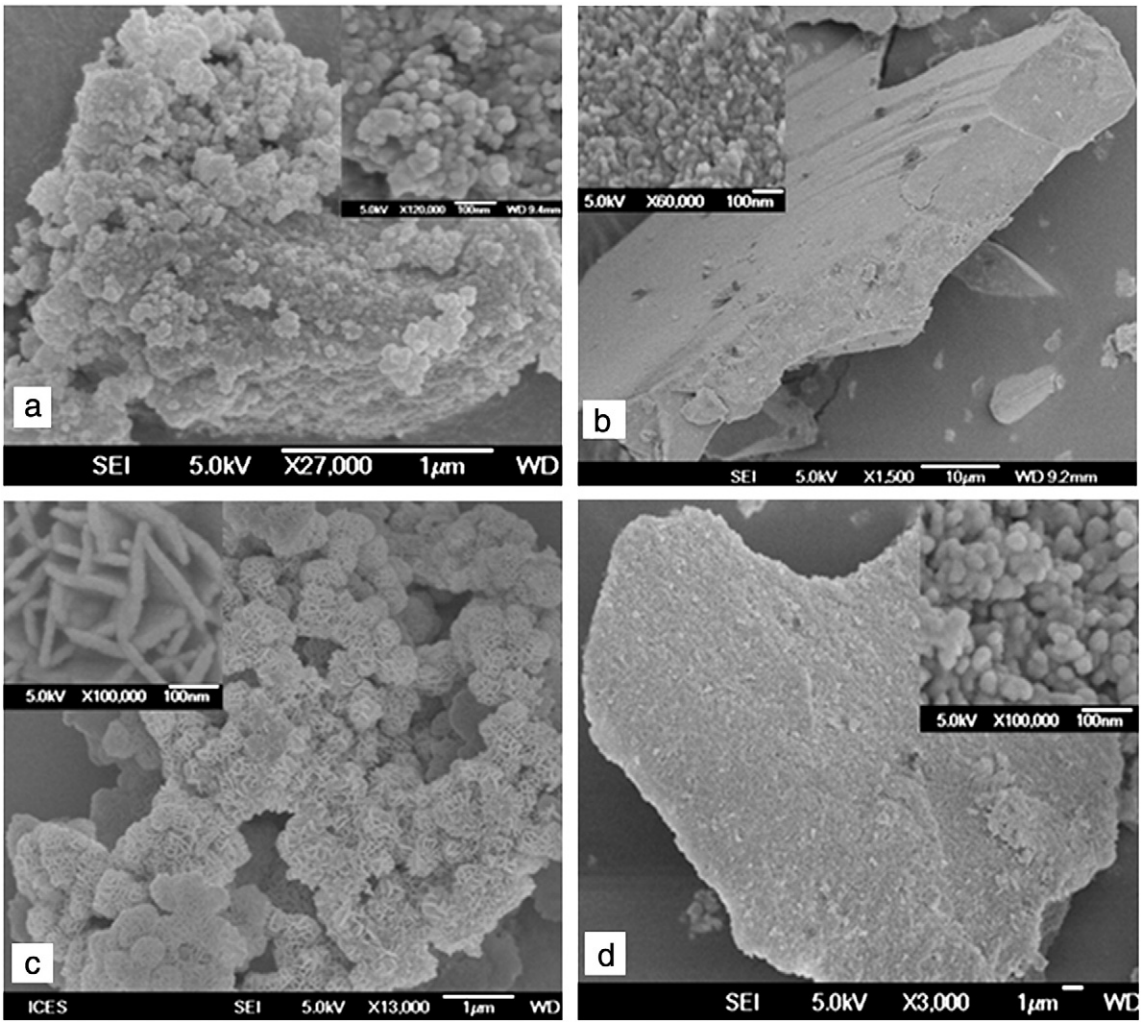

Fig. 6. SEM images of HTs synthesized at (a) pH = 6.5; (b) pH = 9; (c) pH = 10; (d) pH = 14. The insets show the SEM images with higher magnifications.

different from the general HT profiles (Hutson et al., 2004; Ram Reddy et al., 2006). TPD result in Fig. 3 indicated that, at pH 8, γ-AlOOH might still exist since the first H_2O desorption peak was larger than the second. The desorption peaks of CO_2 and NO revealed that both NO_3^- and HCO_3^- were present in the inter-layers as charge compensating anions. For the sample synthesized at pH 9, a thorough characterization (e.g. TGA, DSC, XRD, FTIR, TPD) has been conducted, demonstrating the formation of $Mg_{2.3}Al_1$–HCO_3. It is worthy to mention that the HCO_3^- anion cannot be differentiated from CO_3^{2-} by FTIR analysis. Therefore, a new HT Mg_3Al_1–HCO_3 using a $KHCO_3$ solution (pH was controlled at 8.5) was synthesized. The TGA and DSC profiles of these two samples are compared in Fig. 5. The HT synthesized at pH = 9 showed exactly the same TGA and DSC curves as those of Mg_3Al_1–HCO_3. Particularly, as compared to Mg_3Al_1–CO_3 obtained at pH = 10, the second derivative weight peak and the second heat flow peak of these two samples are much sharper, and the corresponding temperatures are also much higher.

A further increase in pH from 10 to 14 had little influence on the Mg/Al ratios, which kept between 3.1 and 3.2. All characteristic peaks of Mg_3Al_1–CO_3 were detected in their XRD patterns in Fig. 1(a). TGA analyses of all samples showed the typical two-stage profiles (Fig. 2) (Wang et al., 2010a, 2010b). The TPD analyses in Fig. 4 confirmed that the interlayer charge compensating anion was CO_3^{2-}. Therefore, when the pH was equal or higher than 10, all co-precipitation products were HTs having the same chemical composition of Mg_3Al_1–CO_3.

The morphologies of these samples were observed by SEM, as shown in Fig. 6 and Figs. S1–S9. At pH ≤ 8, the particles were formed as an accumulation of primary nano-particles. The morphology is similar to the amorphous γ-AlOOH samples that were synthesized by dripping Al $(NO_3)_3$ into Na_2CO_3 and adjusting pH with NaOH (see Fig. 7). The XRD patterns in Fig. 1(b) also confirm that the products at pH ≤ 8 are mainly γ-AlOOH. At pH 9, very big particles with "stone-like" morphology were formed, which is also very similar to γ-AlOOH synthesized at pH 9 (Fig. 6 (b) and Fig. 7(c)). TGA and DSC analyses in Fig. 5 confirmed that the composition of the hydrotalcite is $Mg_{2.3}Al_1$–HCO_3. This is because the HCO_3^- rather than CO_3^{2-} anions dominated in the solution when the pH is around 9. Like NO_3^- and Cl^-, HCO_3^- is very reactive and able to lead to a fast growth of hydrotalcite (Kameda et al., 2008; Wang et al., 2011a, 2011b). As we have previously reported, Mg–Al–NO_3 and Mg–Al–Cl synthesized using the same method showed similar morphologies (Wang et al., 2011a, 2011b). Their surface areas were also very small, just 8.1 and 10.4 m^2/g, respectively.

At pH 10, "rosette" particles were formed. The formation of this rosette hydrotalcite might be related to its isoelectric point (IEP), which is around 10 (Chang et al., 2007; You et al., 2009). In this condition, although the formation of the primary particles is fast, the growth is slow because the surface of the initially formed primary particles is electrically neutral (pH = IEP). Consequently, the growth of hydrotalcite is preferred along the 001 plane, where the surface charge density is low, resulting in a "rosette" morphology (Li et al., 2007; Luo et al., 2007). At pH ≥ 11, meso-

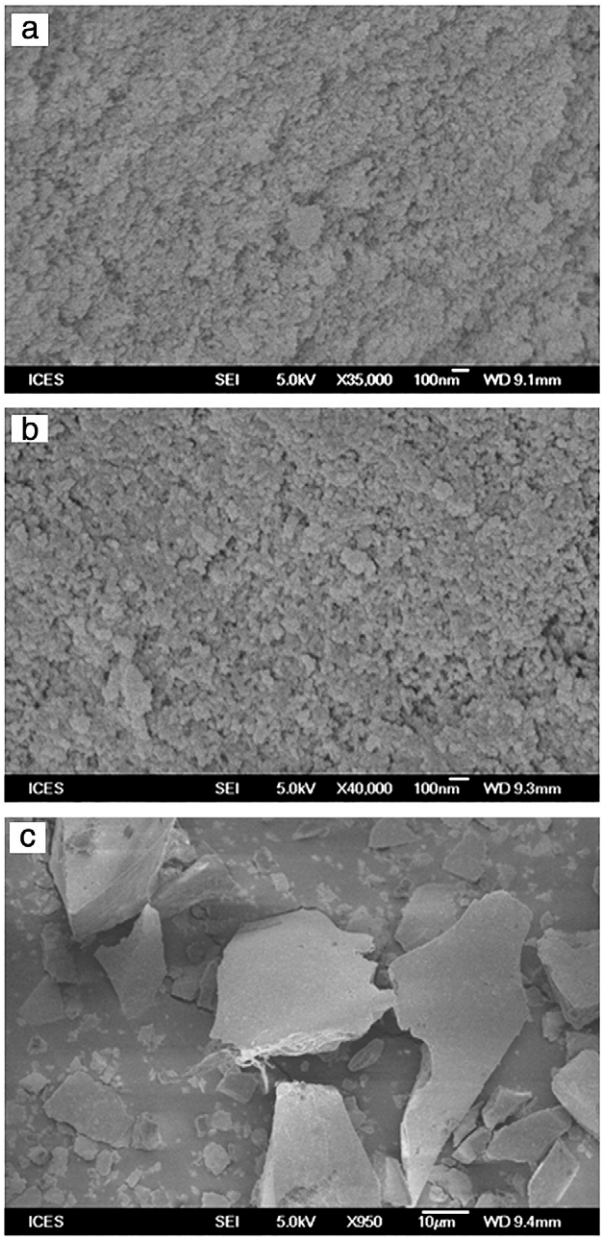

Fig. 7. SEM images of γ-AlOOH synthesized at pH equals (a) 7, (b) 8, and (c) 9.

porous Mg_3Al_1–CO_3 consisting of uniform nano-particles was synthesized (see Fig. 6(d) and Figs. S6–S9). The size of these nanoparticles was around 30 nm. In basic conditions, the formation of HTs was very fast, since the pH value was higher than its IEP, the surface of primarily formed HT nanoparticles was negatively charged. Consequently, any further contact between HT nanoparticles and $Al(OH)_4^-$ (and CO_3^{2-}) was not favored, inhibiting the growth of HTs. The surface areas of the synthesized HTs are thus all around 100 m^2/g. The similar phenomenon has also been observed on the synthesis of $Mg(OH)_2$ by Li et al. (Li et al., 2007) and on the synthesis of β-$Ni(OH)_2$ by Luo et al. (Luo et al., 2007), respectively.

The BET surface area as well as the pore structure were analyzed by N_2 adsorption and desorption isotherms at 77 K (Fig. 8 and Fig. S10). BET surface area first decreased from ~192 to ~14.4 m^2/g with an increase in pH from 6.5 to 9. This is because more MgAl–NO_3 and/or MgAl–HCO_3 were formed with the increase in pH. At pH 6.5–7, the main product was amorphous γ-AlOOH, showing a very high surface area (167–192 m^2/g); while at pH 8–9, the main products were MgAl–NO_3 and/or MgAl–HCO_3, both having very small surface areas. The surface area then increased sharply to 110 m^2/g at pH 10; and a further increase of pH to 14 slightly decreased the BET values. This is because Mg_3Al_1–CO_3, rather than MgAl–NO_3 and MgAl–HCO_3, was formed at pH ≥ 10 and the particle size of the primary nano-particles increased slightly with the increase in pH. The evolution of the average pore size showed another interesting trend with pH. At pH < 10, the average pore size was constant at ~3.7 nm, which was exactly the same as compared to that of the synthesized amorphous γ-AlOOH (see Fig. S11). At pH > 10, the pore size increased with the increase in pH. Interestingly, there are two types of pores at pH 10. The small pore was also 3.7 nm, while the big pore was around 6.3 nm. The relationship between the pore structures and the pH values is discussed in detail later, along with the proposed mechanism.

Based on our investigations, a plausible formation mechanism as a function of the synthesis pH can be proposed. At pH 6.5–9, Al^{3+} first precipitated as γ-AlOOH and Mg^{2+} remained in the solution. Then Mg^{2+} and anions A (A = NO_3^- or HCO_3^-) reacted with γ-AlOOH to form Mg_xAl–A. With the increase of pH values, more Mg_xAl–A will be formed. At pH = 9, pure phase $Mg_{2.3}Al_1$–HCO_3 HT was synthesized. Since the HTs were derived from amorphous γ-AlOOH, the pore size of the synthesized HTs should be similar to that of γ-AlOOH precursor. In these conditions, the interlayer charge compensating anions were NO_3^- and/or HCO_3^-. At pH 10, Al^{3+} and Mg^{2+} had the same chance to be precipitated as $Al(OH)_3$ and $Mg(OH)_2$ nano-particles at the same time, which then immediately converted into Mg_3Al_1–CO_3 HTs. In the next stage, because the surface of the primary Mg_3Al_1–CO_3 nanoparticles is electrically neutral (pH = IEP), the growth of HT was relatively slow and preferentially along the 001 plane. The 001 plane has the lowest surface charge density and thus is stable under the synthesis condition. The growth of the primary nanoparticles into nano-sheets finally resulted in the rosette morphology (see Fig. 9) (Li et al., 2007; Luo et al., 2007). Under this condition, because the HT was derived from both $Al(OH)_3$ and $Mg(OH)_2$, two types of pores may coexist. This mechanism was supported by the BET analyses in Fig. 8 and Fig. S10. At pH 11–14, Mg^{2+} precipitated first as $Mg(OH)_2$, and then immediately converted into Mg_3Al_1–CO_3 nano-particles. Although the formation of HTs was very fast under these basic conditions, its growth was inhibited. According to the IEP theory, the HT surface was negatively charged at pH higher than its IEP. Thus, the interaction between HT nanoparticles and $Al(OH)_4^-$ (and/or CO_3^{2-}, OH^-) was not favored due to the repulsive force. Consequently, mesoporous Mg_3Al_1–CO_3 HTs were obtained under these conditions (see Fig. 9). Table 2 summarizes the Mg/Al ratios, charge compensating anions, morphologies, average pore sizes, and the final products of the samples synthesized at various pH from 6.5 to 14.

It was also proved that this mechanism is applicable to other synthesis methods. For instance, we synthesized Mg_3Al_1–CO_3 at pH 10 and 12 using hydrothermal method. Fig. 10 shows the SEM images of these two samples. At pH 10, the growth of the HT plate was favored and the size was from one to several micrometers. While at pH 12,

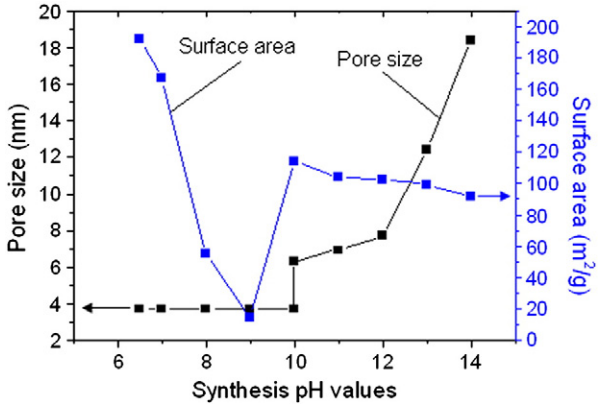

Fig. 8. Pore sizes and surface areas of HTs synthesized at different pHs.

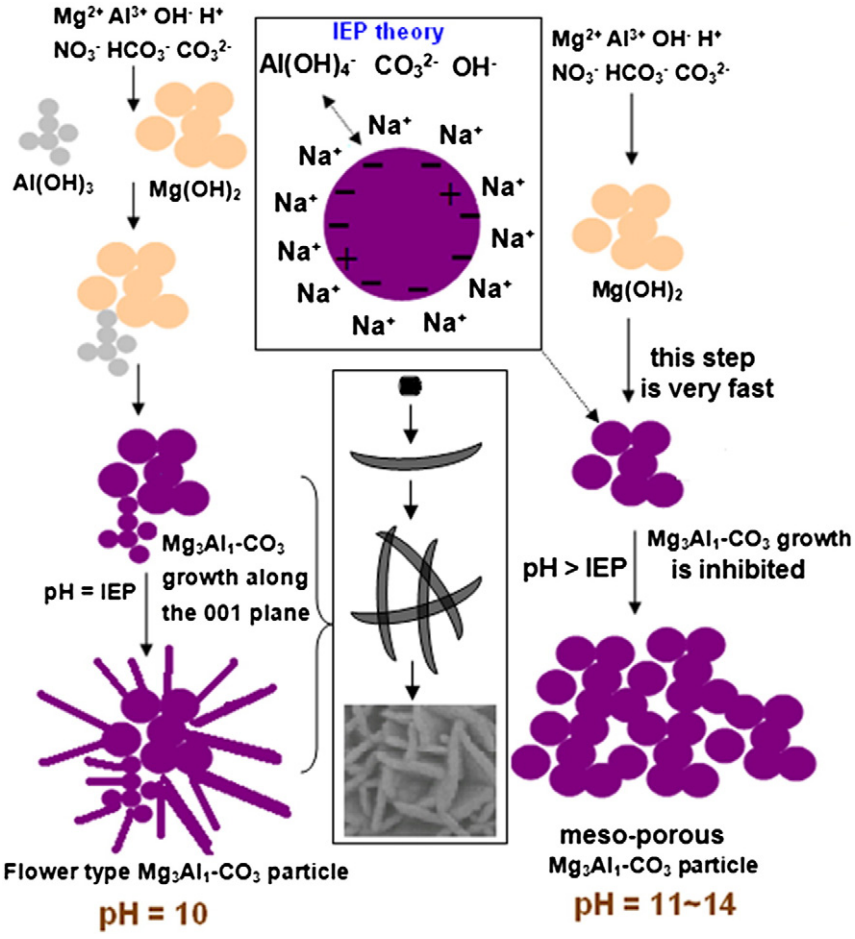

Fig. 9. Proposed synthesis mechanism for Mg–Al HTs at pH 10–14.

because the synthesis pH value was higher than the IEP of Mg_3Al_1–CO_3 and the growth of the particle was inhibited, identical plate-like particles were obtained, with an average size of 200 nm. This result further confirms the proposed synthesis mechanism.

The CO_2 adsorption capacities of Mg_3Al_1–CO_3 HTs synthesized at pH 6.5–14 were then determined as previously indicated. Prior to each adsorption test, fresh HTs were calcined using two different protocols:

Table 2
Summary of the Mg/Al ratios, charge compensating anions, average pore sizes, morphologies, and final products for the samples synthesized at various pH values from 6.5 to 14.

pH	Mg/Al ratio	Anion	Pore size (nm)	Morphology	Final product
6.5	0.5	NO_3^-	3.7	Nano-particle aggregates	γ-AlOOH + Mg_xAl_1–NO_3
7.0	0.6	NO_3^-	3.7	Nanoparticle aggregates	γ-AlOOH + Mg_xAl_1–NO_3
8.0	1.5	NO_3^-/HCO_3^-	3.7	Nanoparticle aggregates	γ-AlOOH + Mg_xAl_1–NO_3/Mg_xAl_1–HCO_3
9.0	2.3	HCO_3^-	3.7	Stone-like	$Mg_{2.3}Al_1$–HCO_3
10.0	3.1	CO_3^{2-}	3.7/6.3	Flower-like	Mg_3Al_1–CO_3
11.0	3.1	CO_3^{2-}	7.2	Flower-like + nanoparticle aggregates	Mg_3Al_1–CO_3
12.0	3.2	CO_3^{2-}	7.6	Nanoparticle aggregates	Mg_3Al_1–CO_3
13.0	3.2	CO_3^{2-}	12.3	Nanoparticle aggregates	Mg_3Al_1–CO_3
14.0	3.2	CO_3^{2-}	18.3	Nanoparticle aggregates	Mg_3Al_1–CO_3

(1) in-situ calcination at 400 °C for 1 h; and (2) ex-situ calcination at 400 °C for 5 h, immediately followed by in-situ calcination at 400 °C for 1 h. After pretreatment, the samples were cooled down to the adsorption temperature (200 °C) and held at that temperature for 0.5 h for stabilization purpose. The feed gas was then switched to CO_2 for adsorption. Fig. 11 indicates that the CO_2 adsorption capacities were very low when pH was lower than 10. Particularly at pH 6.5 and 7, although the BET surface areas were very high (ca. 165–190 m^2/g, see Fig. 8), the Mg/Al ratio was too low to have sufficient Mg–O sites for CO_2 adsorption. Only a very small amount of CO_2, ca. 0.06–0.08 mmol/g was adsorbed on these samples. All HTs synthesized at pH 10–14 showed much better performance for capturing CO_2, which might be attributed to the well formation of Mg_3Al_1–CO_3. The substitution of Mg^{2+} by Al^{3+} creates plenty of active Mg–O sites on the surface. The highest CO_2 capture capacity was observed at pH 12. After being pre-calcined at 400 °C for 1 h and 6 h, the CO_2 capture capacity was 0.83 and 0.58 mmol/g, respectively. Our experiments indicated that further increasing the pre-calcination time has no influence on the CO_2 capture capacity. At pHs 13 and 14, the CO_2 adsorption capacity slightly decreased, which might be due to the decrease of surface area.

4. Conclusions

In summary, this work reveals that the synthesis pH plays a crucial role on the morphology, pore structure as well as the chemical composition of HTs. At pH < 9, the product is mainly γ-AlOOH coexisting with certain amount of Mg–Al–NO_3 and/or Mg–Al–HCO_3 HT; at pH = 9, the product is a "stone-like" HT with a composition of $Mg_{2.3}Al_1$–HCO_3; at pH = 10, the product is a "rosette" HT with a composition of Mg_3Al_1–CO_3; while at pH > 10, the products are mesoporous HTs with a

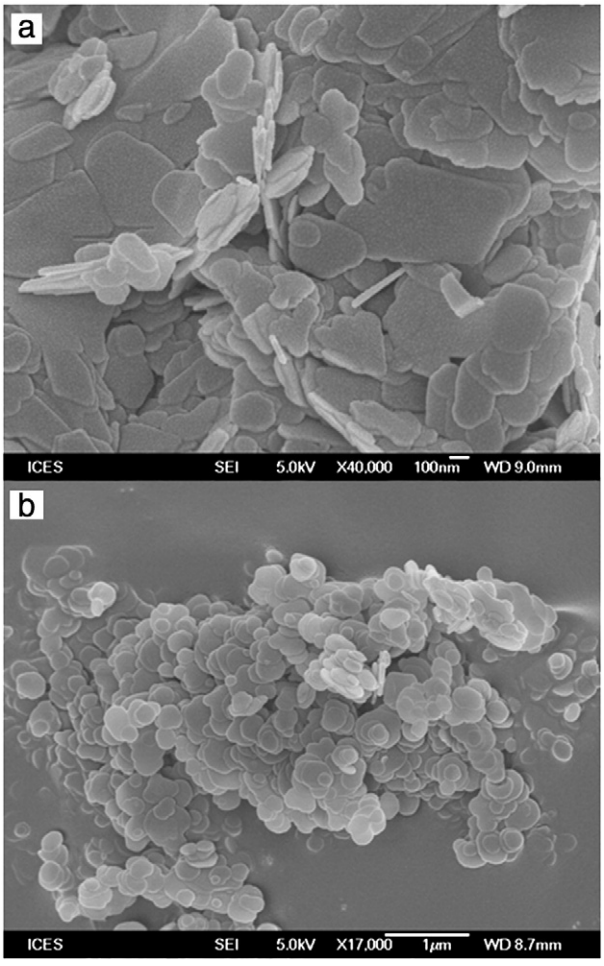

Fig. 10. SEM images of (a) Mg_3Al_1–CO_3 pH 10, and (b) Mg_3Al_1–CO_3 pH 12 synthesized at 150 °C by hydrothermal synthesis method.

composition of Mg_3Al_1–CO_3. At pH<10, the pore size is constant at ~3.7 nm, while at pH>10, the pore size increases with the increase in pH. Interestingly there are two types of pores at pH = 10. Based on our observations, the plausible synthesis mechanism is proposed, which not only describes the formation process under various synthesis conditions, but also explains the morphology and pore structure of the resulting HTs. In this mechanism, the relationship between synthesis pH and the IEP of HTs determines the morphology of the final products. The proposed formation mechanism is further verified by hydrothermal synthesis method. CO_2 adsorption studies indicate that both the physical and chemical properties of HTs influence their CO_2 capture capacity. In order to have a good CO_2 adsorption capacity, the synthesis pH should be equal or higher than 10. Among all samples, Mg_3Al_1–CO_3 (pH 12) shows the highest CO_2 capture capacity of 0.83 mmol/g (pre-calcined for 1 h) and 0.58 mmol/g (pre-calcined for 6 h).

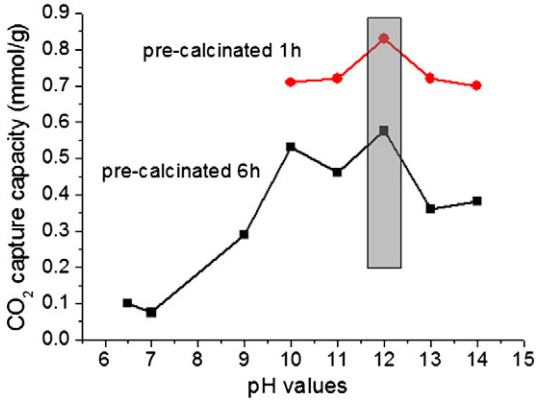

Fig. 11. CO_2 capture capacities of HTs synthesized with different pH values from 6.5 to 14. Prior to CO_2 adsorption, fresh HTs were first pretreated at 400 °C for 1 h or 6 h.

Acknowledgment

This work is financially supported by the Thematic Strategic Research Program (Grant nos. 0921380024) from the Agency for Science, Technology and Research (A*STAR) of Singapore.

Appendix A. Supplementary data

Electronic supplementary information (ESI) available: SEM images and pore size distributions of HTs synthesized at pH = 6.5–14; pore size distributions of γ-AlOOH synthesized at pH = 7, 8, 10. Supplementary data to this article can be found online at doi:10.1016/j.clay.2011.07.024.

References

Benito, P., Labajos, F.M., Rives, V., 2006. Uniform fast growth of hydrotalcite-like compounds. Cryst. Growth Des. 6, 1961–1966.
Benito, P., Guinea, I., Herrero, M., Labajos, F.M., Rives, V., 2007. Incidence of microwave hydrothermal treatments on the crystallinity properties of hydrotalcite-like compounds. Z. Anorg. Allg. Chem. 633, 1815–1819.
Benito, P., Guinea, I., Labajos, F.M., Rives, V., 2008. Microwave-assisted reconstruction of Ni,Al hydrotalcite-like compounds. J. Solid State Chem. 181, 987–996.
Benito, P., Herrero, M., Labajos, F.M., Rives, V., 2010. Effect of post-synthesis microwave-hydrothermal treatment on the properties of layered double hydroxides and related materials. Appl. Clay Sci. 48, 218–227.
Boclair, J.W., Braterman, P.S., 1999. Layered double hydroxide stability. 1. Relative stabilities of layered double hydroxides and their simple counterparts. Chem. Mater. 11, 298–302.
Boclair, J.W., Braterman, P.S., Jiang, J., Lou, S., Yarberry, F., 1999. Layered double hydroxide stability. 2. Formation of Cr(III)-containing layered double hydroxides directly from solution. Chem. Mater. 11, 303–307.
Cavani, F., Trifirò, F., Vaccari, A., 1991. Hydrotalcite-type anionic clays: preparation, properties and applications. Catal. Today 11, 173–301.
Chang, C.T., Liaw, B.J., Huang, C.T., Chen, Y.Z., 2007. Preparation of Au/Mg_xAlO hydrotalcite catalysts for CO oxidation. Appl. Catal. A: Gen. 332, 216–224.
Chen, X.Y., Zhang, Z.J., Li, X.L., Lee, S.W., 2008. Controlled hydrothermal synthesis of colloidal boehmite (γ-AlOOH) nanorods and nanoflakes and their conversion into γ-Al_2O_3 nanocrystals. Solid State Commun. 145, 368–373.
Climent, M.J., Corma, A., Iborra, S., Epping, K., Velty, A., 2004. Increasing the basicity and catalytic activity of hydrotalcites by different synthesis procedures. J. Catal. 225, 316–326.
Climent, M.J., Corma, A., Frutos, P.D., Iborra, S., Noy, M., Velty, A., Concepción, P., 2010. Chemicals from biomass: synthesis of glycerol carbonate by transesterification and carbonylation with urea with hydrotalcite catalysts. The role of acid–base pairs. J. Catal. 269, 140–149.
Costantino, U., Marmottini, F., Nocchetti, M., Vivani, R., 1998. New synthetic routes to hydrotalcite-like compounds — characterization and properties of the obtained materials. Eur. J. Inorg. Chem. 10, 1439–1446.
Costantino, U., Nocchetti, M., Sisani, M., Vivani, R., 2009. Recent progress in the synthesis and application of organically modified hydrotalcites. Z. Kristallogr. 224, 273–281.
Du, Y., O'Hare, D., 2008. Synthesis, morphology, structure, and magnetic characterization of layered cobalt hydroxyisocyanates. Inorg. Chem. 47, 3234–3242.
Herrero, M., Labajos, F.M., Rives, V., 2009. Size control and optimisation of intercalated layered double hydroxides. Appl. Clay Sci. 42, 510–518.
Hibino, T., Ohya, H., 2009. Synthesis of crystalline layered double hydroxides: precipitation by using urea hydrolysis and subsequent hydrothermal reactions in aqueous solutions. Appl. Clay Sci. 45, 123–132.
Hu, G., Wang, N., O'Hare, D., Davis, J., 2007. Synthesis of magnesium aluminium layered double hydroxides in reverse microemulsions. J. Mater. Chem. 17, 2257–2266.
Hutson, N.D., Attwood, B.C., 2008. High temperature adsorption of CO_2 on various hydrotalcite-like compounds. Adsorption 14, 781–789.
Hutson, N.D., Speakman, S.A., Payzant, E.A., 2004. Structural effects on the high temperature adsorption of CO_2 on a synthetic hydrotalcite. Chem. Mater. 16, 4135–4143.
Kagunya, W., Hassan, Z., Jones, W., 1996. Catalytic properties of layered double hydroxides and their calcined derivatives. Inorg. Chem. 35, 5970–5974.
Kameda, T., Yoshioka, T., Yabuuchi, F., Uchida, M., Okuwaki, A., 2008. Effects of pH and concentration on ability of Cl^- and NO_3^- to intercalate into a hydrotalcite-like compound during its synthesis. Bull. Mater. Sci. 31, 625–629.

Komarneni, S., Li, Q.H., Roy, R., 1996. Microwave-hydrothermal processing of layered anion exchangers. J. Mater. Res. 11 1866–1839.
Kovanda, F., Grygar, T., Dornicak, V., 2003. Thermal behaviour of Ni–Mn layered double hydroxide and characterization of formed oxides. Solid State Sci. 5, 1019–1026.
Labajos, F.M., Rives, V., Ulibarri, M.A., 1992. Effect of hydrothermal and thermal treatments on the physicochemical properties of Mg–Al hydrotalcite-like materials. J. Mater. Sci. 27, 1546–1552.
Li, Q., Liu, H., Lu, H., Zheng, M., Xie, J., Chen, Y., 2007. Effects of pH on the growth of Mg $(OH)_2$ crystals. J. Mater. Sci. Eng. 25, 609–619.
Luo, Y., Duan, G., Li, G., 2007. Synthesis and characterization of flower-like β-$Ni(OH)_2$ nanoarchitectures. J. Solid State Chem. 180, 2149–2153.
Ma, R., Takada, K., Fukuda, K., Iyi, N., Bando, Y., Sasaki, T., 2008. Topochemical synthesis of monometallic $(Co^{2+}–Co^{3+})$ layered double hydroxide and its exfoliation into positively charged $Co(OH)_2$ nanosheets. Angew. Chem. Int. Ed. 47, 86–89.
Manzi-Nshuti, C., Wang, D., Hossenlopp, J.M., Wilkie, C.A., 2008. Aluminum-containing layered double hydroxides: the thermal, mechanical, and fire properties of (nano) composites of poly(methyl methacrylate). J. Mater. Chem. 18, 3091–3102.
Montanari, T., Sisani, M., Nocchetti, M., Vivani, R., Concepcion Herrera Delgado, M., Ramis, G., Busca, G., Costantino, U., 2010. Zinc-aluminum hydrotalcites as precursors of basic catalysts: preparation, characterization and study of the activation of methanol. Catal. Today 152, 104–109.
Nyambo, C., Songtipya, P., Manias, E., Jimenez-Gasco, M.M., Wilkie, C.A., 2008. Effect of MgAl-layered double hydroxide exchanged with linear alkyl carboxylates on fire-retardancy of PMMA and PS. J. Mater. Chem. 18, 4827–4838.
Oliveira, E.L.G., Grande, C.A., Rodrigues, A.E., 2008. CO_2 sorption on hydrotalcite and alkali-modified (K and Cs) hydrotalcites at high temperatures. Sep. Purif. Technol. 62, 137–147.
Paredes, S.P., Fetter, G., Bosch, P., Bulbulian, S., 2006. Sol–gel synthesis of hydrotalcite — like compounds. J. Mater. Sci. 41, 3377–3382.
Perez-Ramirez, J., Abello, S., van der Pers, N.M., 2007. Memory effect of activated Mg–Al hydrotalcite: in situ XRD studies during decomposition and gas-phase reconstruction. Chem. Eur. J. 13, 870–878.
Ram Reddy, M.K., Xu, Z.P., Lu, G.Q., Diniz da Costa, J.C., 2006. Layered double hydroxides for CO_2 capture: structure evolution and regeneration. Ind. Eng. Chem. Res. 45, 7504–7509.
Reijers, H.Th.J., Valster-Schiermeier, S.E.A., Cobden, P.D., van den Brink, R.W., 2006. Hydrotalcite as CO_2 sorbent for sorption-enhanced steam reforming of methane. Ind. Eng. Chem. Res. 45, 2522–2530.
Seron, A., Delorme, F., 2008. Synthesis of layered double hydroxides (LDHs) with varying pH: A valuable contribution to the study of Mg/Al LDH formation mechanism. J. Phys. Chem. Solids 69, 1088–1090.
Takagaki, A., Iwatani, K., Nishimura, S., Ebitani, K., 2010. Synthesis of glycerol carbonate from glycerol and dialkyl carbonates using hydrotalcite as a reusable heterogeneous base catalyst. Green Chem. 12, 578–581.
Tamura, H., Chiba, J., Ito, M., Takeda, T., Kikkawa, S., Mawatari, Y., Tabata, M., 2006. Formation of hydrotalcite in aqueous solutions and intercalation of ATP by anion exchange. J. Colloid Interface Sci. 300, 648–654.
Tsujimura, A., Uchida, M., Okuwaki, A., 2007. Synthesis and sulfate ion-exchange properties of a hydrotalcite-like compound intercalated by chloride ions. J. Hazard. Mater. 143, 582–586.
Venugopal, A., Palgunadi, J., Deog, J.K., Joo, O.S., Shin, C.H., 2009. Hydrotalcite derived Cu–Zn–Cr catalysts admixed with γ-Al_2O_3 for single step dimethyl ether synthesis from syngas: influence of hydrothermal treatment. Catal. Today 147, 94–99.
Wang, L., Su, S., Chen, D., Wilkie, C.A., 2009. Variation of anions in layered double hydroxides: effects on dispersion and fire properties. Polym. Degrad. Stab. 94, 770–781.
Wang, J., Li, D., Yu, X., Zhang, M., Jing, X., 2010a. Fabrication of layered double hydroxide spheres through urea hydrolysis and mechanisms involved in the formation. Colloid Polym. Sci. 288, 1411–1418.
Wang, Q., Tay, H.H., Ng, D.J.W., Chen, L., Liu, Y., Chang, J., Zhong, Z., Luo, J., Borgna, A., 2010b. The effect of trivalent cations on the performance of Mg–M–CO_3 layered double hydroxides for high-temperature CO_2 capture. ChemSusChem 3, 965–973.
Wang, Q., Luo, J., Zhong, Z., Borgna, A., 2011a. CO_2 capture by solid adsorbents and their applications: current status and new trends. Energy Environ. Sci. 4, 42–55.
Wang, Q., Wu, Z., Tay, H.H., Chen, L., Liu, Y., Chang, J., Zhong, Z., Luo, J., Borgna, A., 2011b. High temperature adsorption of CO_2 on Mg–Al hydrotalcite: effect of the charge compensating anions and the synthesis pH. Catal. Today 164, 198–203.
Xu, Z.P., Lu, G.Q., 2005. Hydrothermal synthesis of layered double hydroxides (LDHs) from mixed MgO and Al_2O_3: LDH formation mechanism chem. Mater. 17, 1055–1062.
You, K.J., Chang, C.T., Liaw, B.J., Huang, C.T., Chen, Y.Z., 2009. Selective hydrogenation of α, β-unsaturated aldehydes over Au/MgxAlO hydrotalcite catalysts. Appl. Catal. A: Gen. 361, 65–71.